Structural Engineering and Mechanics, *Vol. 74, No. 3 (2020) 395-406*
DOI: https://doi.org/10.12989/sem.2020.74.3.395

Research on prefabricated concrete beam-column joint with high strength bolt-end plate

Li Shufeng*[1], Zhao Di[1], Li Qingning[2], Zhao Huajing[3], Zhang Jiaolei[2] and Yuan Dawei[2]

[1]*School of Traffic and Transportation of Xu'chang University, Xu'chang, Henan, 461000, China*
[2]*School of Civil Engineering of Xi'an University of Architecture and Technology, Xi'an, Shanxi, 710055, China*
[3] *School of Science of Xi'an University of Architecture and Technology, Xi'an, Shanxi, 710055, China*

(Received October 28, 2019, Revised December 11, 2019, Accepted December 14, 2019)

Abstract. Many prefabricated concrete frame joints have been proposed, and most of them showed good seismic performance. However, there are still some limitations in the proposed fabricated joints. For example, for prefabricated prestressed concrete joints, prefabricated beams and prefabricated columns are assembled as a whole by the pre-stressed steel bar and steel strand in the beams, which brings some troubles to the construction, and the reinforcement in the core area of the joints is complex, and the mechanical mechanism is not clear. Based on the current research results, a new type of fabricated joint of prestressed concrete beams and confined concrete columns is proposed. To study the seismic performance of the joint, the quasi-static test is carried out. The test results show that the nodes exhibit good ductility and energy dissipation. According to the experimental fitting method and the "fixed point pointing" law, the resilience model of this kind of nodes is established, and compared with the experimental results, the two agree well, which can provides a certain reference for elasto-plastic seismic response analysis of this type of structure. Besides, based on the analysis of the factors affecting the shear capacity of the node core area, the formula of shear capacity of the core area of the node is proposed, and the theoretical values of the formula are consistent with the experimental value.

Keywords: prefabricated joint; seismic performance; resilience model; shear capacity; node core area

1. Introduction

At present, China's construction industry is in the stage of transformation and upgrading, and prefabricated building, as the carrier of the transformation and upgrading of the traditional construction industry in our country, is being vigorously promoted. Developing prefabricated buildings is a transformation of construction methods, a progress of social productivity, and an evolution of social forms. Fabricated building can be assembled into a whole building by prefabricating part or all of the components of the building in the factory, then transporting them to the construction site, and finally using reliable connections to combine the components, which shows the advantages of good quality, shortening of the construction period and resources saving. In China, concrete construction still occupies a dominant position, fabricated concrete buildings not only inherit the advantages of durability and stability of cast-in-situ concrete buildings, but also save more resources and have better environmental protection compared with traditional cast-in-situ concrete, which is in line with the current green building development model advocated by China. At present, scholars at home and abroad have proposed a number of new fabricated joints and prefabricated prestressed concrete frame joints, and the seismic performance of fabricated joints is very close to that of cast-in-place concrete joints (Parastesh, H. *et al*. 2014, Mohammad, Y. *et al*. 2016, Rattapon, K. and Chayanon, H. 2018, Fan, L. 2010, Li, X.M *et al*. 2013, Cheng, P *et al*. 2015, Liu, R.R. 2015, Liao, X.D. 2016, Yu, J.B. and Guo, Z.X. 2017). However, these fabricated nodes still have certain limitations. For example, for prefabricated prestressed concrete joints, the beam and column are assembled through the prestressed steel bars and steel strands in the beam, and the prestressed steel bars and steel strands pass through the core area of the joint, which brings certain troubles to the construction and the mechanism of the force is not clear. To improve this situation, the bolt end plate connection used in the steel structure and composite structure is extended to concrete structure(Zhang, X.H. *et al*. 2014, Peng, Z. *et al*. 2016, He, Y.B. *et al*. 2012), a new type of assembled joints of prestressed concrete beams and confined concrete columns connected by high strength bolt end plates is presented in this paper.

2. Basic structure of fabricated beam-column joint

From the existing research results, bolted end-plate connections show better seismic performance. In this paper, end-plate bolt connection is applied in concrete structure. To avoid the prestressed reinforcement passing through the core area of the joint, prestressed reinforcement passing through the anchor plate is anchored inside the end plate by nut, and the end plate and the anchor plates are welded together by groove welding. The non-prestressed

*Corresponding author, Ph.D.
E-mail: 1371757493@qq.com

ISSN: 1225-4568 (Print), 1598-6217 (Online)

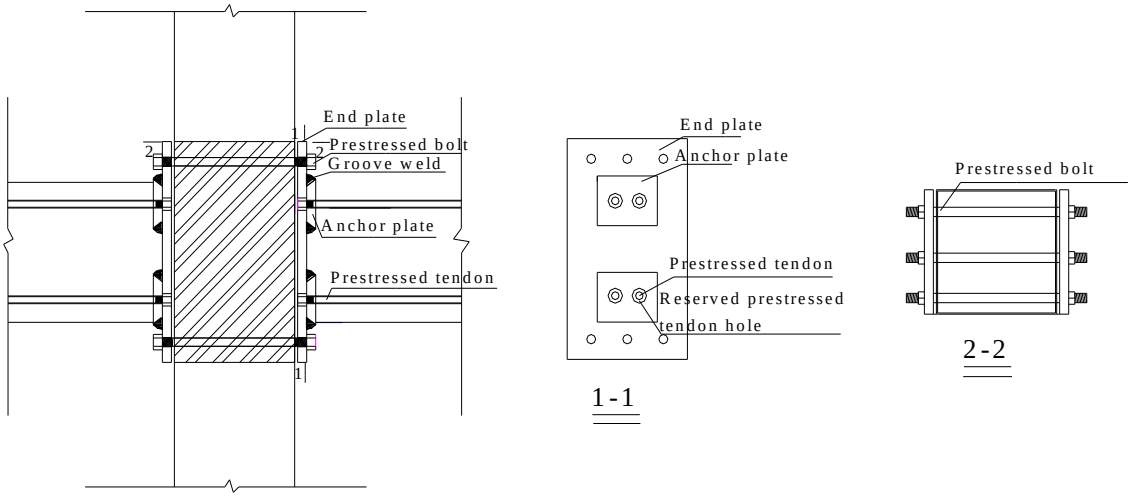

Fig. 1 The detail figures of connection

(a) 2 bolt rows configuration (b) 4 bolt rows configuration

Fig. 2 The configurations of high-strength bolt end joints

reinforcements are welded on the end plate by the expanded pier head, which can guarantee the quality of the connection between the nonprestressed tendons and the end plate. In addition, in order to increase the stiffness and shear strength, stirrups are replaced by the steel plate hoop with the thickness of 4mm in joint zone. To ensure the synergistic work of the steel hoop and the concrete, the reinforcement bar should be welded inside the steel plate hoop. The concrete beams are connected to column by end-plates and six high-strength bolts passing through the core area, the size of end plate is 400mm×30mm×710mm and the diameter of Grade HTH1080 bolts is 27mm. The Grade HTH1100 spiral stirrups are used in the beam and column, and the diameter of spiral stirrup used is 5mm. The advantages of the prefabricated concrete joint with high strength bolt end plate are that force mechanism is clear, construction is convenient, and complicated situation of the reinforcing bars in the core area of the joint is avoided. The detail figures of connection can be seen in Fig. 1.

3. Design criteria for high strength bolt end plate joints

The bolt end plate connection applied to steel structures is extended to concrete structures, so the design criteria of this type of joint are similar to those of the steel structure. According to relevant literature and domestic and foreign codes, the design criteria for high strength bolt end plate joints is given. For the high-strength bolt end plate connection, the pretension applied by the high-strength bolt meets formula (1), the beam column joint can be considered as rigid joint(CECS:2013. 2013).

$$P = 0.7A_e f_y^u \tag{1}$$

Where P is the pretension of the high-strength bolt; A_e is the effective cross-sectional area of the high-strength bolt. $f u$ y is the ultimate tensile strength of the high-strength bolt.

To achieve the design criteria of "strong connection and weak member", the flexural strength of connections M_n is not less than the bending moment at column face M_f due to the probable maximum moment developed by the plastic hinge of the connected beam (AISC. 2016, Tartaglia R., D'Aniello M. and Rassati G.A. 2019), namely

$$M_n \geq M_f = M_{pr} + V_u \bullet S_h \tag{2}$$

$$V_u = 2M_{pr} / L_h + V_{gravity} \tag{3}$$

Where M_f is the bending moment at column face; M_{pr} is the probable maximum moment at plastic hinge; V_u is the shear force acting into the section where the plastic hinge forms. S_h is distance from the face of the column to the

Table 1 Arrangement of reinforcement of specimen

Specimen	Strength of Concrete	Section Type	Section Size (mm)	Longitudinal Reinforcement	Stirrup Spacing (mm)	Stirrup Encryption Area (mm)
column	C40	rectangle	400×400	16Φ22HRB600	50	30
#PAN-01	C35				110	90
#PAN-03	C35				60	50
#PAN-04	C35				70	60
#PAN-05	C35	rectangle	450×200	4Φ20HTH1080	90	70
#PAN-07	C35			4Φ18HRB400	90 (double stirrup)	70 (double stirrup)
#PAN-08	C35				100 (double stirrup)	80 (double stirrup)

plastic hinge; L_h is the distance between plastic hinges and $V_{gravity}$ is the shear force due to gravity loads.

The bolt distance is determined according to the code of steel structures(GB50017-2017, 2017), taking 2 bolt rowand 4 bolt row for example, the configurations of the bolts are shown in Fig. 2.

The minimum diameter for bolts are given as follows (Tartaglia R., D'Aniello M., Rassati G.A. *et al*. 2018, AISC. 2016)

$$d_{b,required} = \sqrt{\frac{\frac{4}{3}M_f}{\pi\phi_n F_{nt} h_0}} \text{(for 2 bolt rows configuration)} \quad (4)$$

$$d_{b,required} = \sqrt{\frac{2M_f}{\pi\phi_n F_{nt}(h_0+h_1)}} \text{(for 4 bolt rows configuration)} \quad (5)$$

Where F_{nt} is the nominal tensile strength of a bolt; h_i is the distance from the centerline of the beam compression zone to the centerline of the i-th tension bolt row; h_0 is distance from the centerline of the compression flange to the tension-side outer bolt row.

According to the code for design of steel structures (GB50017-2017, 2017), the bearing capacity of high-strength bolt under the combined action of tension and shear can be expressed as:

$$\frac{N_t}{N_t^b} + \frac{N_v}{N_v^b} \le 1 \quad (6)$$

Where N_t^b and N_v^b are the nominal tensile and shear strength of the bolts, respectively, and N_t and N_v are the relevant forces acting on the bolt.

The value of N_t^b can be calculated as follows:

$$N_t^b = 0.8P \quad (7)$$

Where P is the pretension of high-strength bolt.

The value of N_v^b is given by

$$N_v^b = 0.9 n_f \mu P \quad (8)$$

Where n_f is the number of friction surfaces; μ is the anti-sliding coefficient of the friction surface.

The minimum thickness of the end-plate is obtained as(Tartaglia R., D'Aniello M., Rassati G.A. *et al*, 2018, AISC.2016)

$$t_{p,required} = \sqrt{\frac{1.11M_f}{\phi_d F_{yp} Y_c}} \quad (9)$$

Where F_{yp} is the specified minimum yield stress of the end-plate material; Y_P is the end-plate yield line mechanism parameter given from AISC358–16(AISC. 2016). F_{yc} is the specified minimum yield stress of the column flange material; ϕ_d is the resistance factor for ductile limit state, which is equal to 1.00.

In this test, eight specimens were designed, the number of the specimen is #PAN-01~#PAN-08. But the quasi-static test of #PAN-02 and #PAN-06 not completed because of equipment factors, and they are not mentioned in this paper. The prefabricated beam and prefabricated column are connected by six HTH1080 high strength screw with a diameter of 28 mm. The section size of the end plate is 30mm×400mm×710mm(t×b×h). The HTH1100 high strength continuous spiral stirrups with diameter of 5 mm are adopted in beams and columns. The double stirrup confined concrete beams are used in the specimens #PAN-07 and #PAN-08. The basic parameters of specimens are shown in Table 1. The fabrication process of the specimen is shown in Fig. 3. The whole production process is completed in the laboratory. It can be seen from the whole process that the fabrication and assembly of prefabricated beams and columns can be fully realized.

4. Discussion on experimental results

Under the action of quasi-static test, it can be seen from the failure phenomena of the specimens that the typical bending failure of beam end happened in all fabricated specimens, and plastic hinge is fully developed. Besides, no fracture and sealing off occur at the enlarged pier head of non-prestressed reinforcement and end-plate. The cracking load and ultimate load of specimens #PAN-07 and #PAN-08 are relatively high, and specimens #PAN-07 and #PAN-08 have small damage region, which indicates that double-layer stirrups have a remarkable impact on concrete core.

(a) Reinforcement skeleton of column

(b) Steel plate hoop

(c) The steel plate hoop replace common stirrup in joint zone

(d) Reinforcement skeleton of precast beam

(e) The prestressed reinforcements are anchored inside the end plate by nut

(f) Assembly of components

Fig. 3 The fabrication and assembly process of specimens

(a) #PAN-05 ultimate failure diagram

(b) #PAN-08 ultimate failure diagram

Fig. 4 Specimens ultimate failure modes

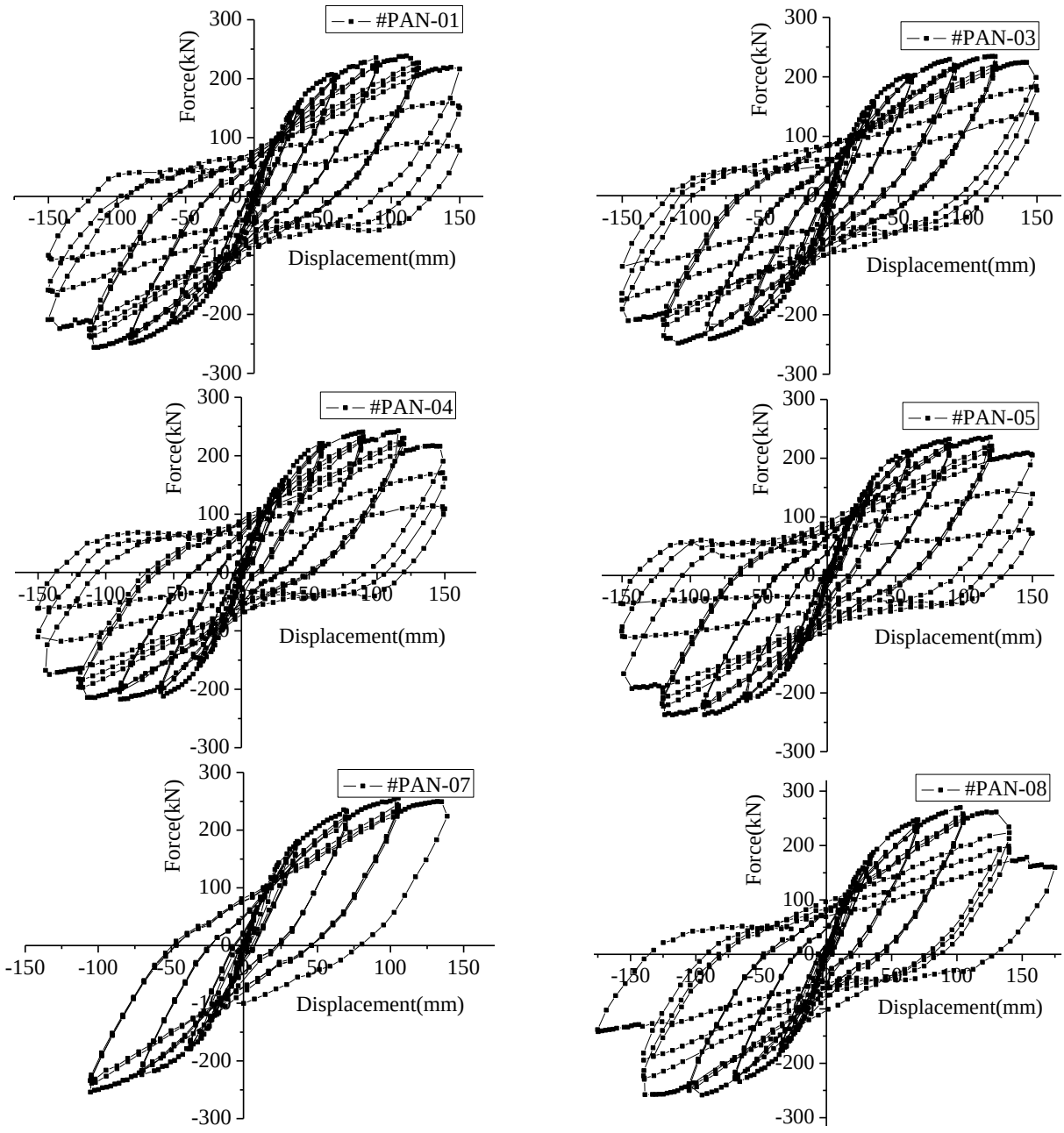

Fig. 5 Hysteretic curve of specimens

The failure modes of single-layer stirrup specimens and double-layer stirrup specimens are shown in Fig. 4. The force-displacement hysteresis curves and skeleton curves for all specimens can be seen in Fig. 5 and Fig. 6, respectively. It can be seen from the hysteretic curves that the hysteretic curves of all specimens show similar characteristics due to the plastic hinge failure at the end of the beam. During initial stage of loading, there is almost no residual deformation. In the later stage of loading, the specimens show a slight pinching phenomenon. After entering the displacement control stage, under the increase of large displacement, the load increases slowly and the stiffness deteriorates to a certain extent. However, under the same level of control displacement, the three-cycle curve is basically close, and the strength and stiffness degradation are not obvious. As can be seen from Fig. 6, the skeleton curves of all fabricated node specimens under horizontal low-cycle reciprocating loads are approximately the same, and they all undergo four stages: elasticity, yield, strengthening and descent. The yield strength and ultimate bearing capacity of specimens #PAN-07 and #PAN-08 are higher than those of specimens, which indicates that double-layer stirrup can better constrain the concrete beam. To quantitatively analyze the seismic performance of the joint, the equivalent viscosity coefficient and ductility of prefabricated node can be obtained according to the hysteresis curve and the skeleton curve. The equivalent viscous coefficient of each prefabricated node is between 0.22 and 0.24(Zeng, L. 2008, Wang, L. *et al.* 2014), and the ductility coefficient of the prefabricated nodes is between

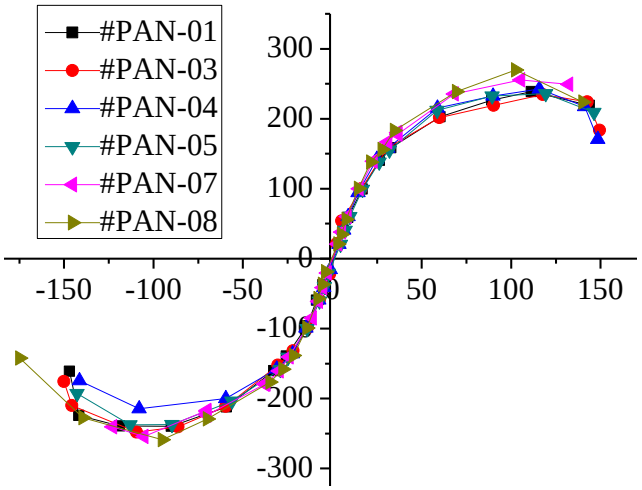

Fig. 6 Skeleton curve of specimen

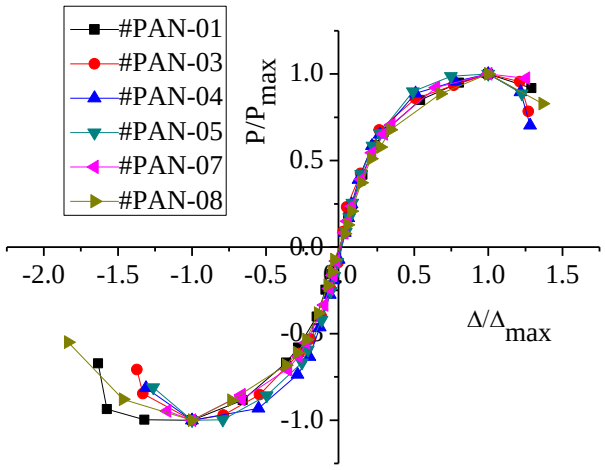

Fig. 7 The dimensionless skeleton curve of the specimen

Table 2 Skeleton curve equation

Line segment	Regression equation	Angle with horizontal axis
OA	$y = 2.412x$	67°
AB	$y = 0.486x + 0.514$	26°
BC	$y = -0.345x + 1.345$	-19°
OA’	$y = 2.259x$	66°
A’B’	$y = 0.356x - 0.644$	20°
B’C’	$y = 0.425x - 1.425$	-23°

2.5 and 3.4(Zenunović, D. and Folić R. 2012), which indicates that the prefabricated node exhibit better energy dissipation and deformability.

5. Establishment of restoring force model of fabricated beam-column joints

Because the factors affecting the restoring force characteristics of the fabricated joint with high-strength bolt-end plate are complex, it is difficult to establish the restoring force model by theoretical method. The hysteretic curve and skeleton curve obtained from the quasi-static test are summarized and simplified, and the restoring force model of the fabricated joint is established. The skeleton curve is processed with dimensionless treatment, the abscissa is represented by Δ/Δ_y, and the longitudinal coordinate is represented by P/P_{max}. The results of dimensionless skeleton curve are shown in Fig. 7. As can be seen from Fig. 7, the trend of dimensionless skeleton curve is basically the same, and the characteristic points are basically the same. Therefore, the skeleton curve can adopt the trilinear model with stiffness degradation (Chen, W.W. and Li, S.C. 2014, Guan, D.Z. *et al*. 2018). The key points are yield displacement Δ_y, yield load P_y, limit displacement Δ_{max}, limit load P_{max}, failure displacement Δ_u and failure load P_u. According to linear regression, a unified skeleton curve model can be obtained, which can be seen in Fig. 8. The regression formulas of each segment are shown in Table 2.

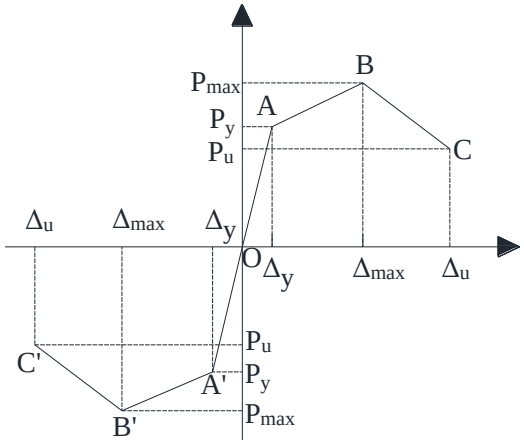

Fig. 8 Three-fold line model

5.1 Comparison of skeleton curve

According to the restoring force model, the simulation results of this paper and the literature (Jiang, H.T. *et al*. 2016) are compared with the test results. The comparison results are shown in Fig. 9. From Fig. 9, the proposed trilinear skeleton curve of restoring force is basically consistent with the test curve.

5.2 Hysteretic principle

The restoring force model of fabricated concrete beams and columns under low cyclic repeated loading shows the rule of “fixed point pointing”. The location of the fixed point is approximately the intersection of the positive (reverse) loading curve and the initial curve. The positive(reverse) longitudinal coordinates of the fixed point are $0.5P_{max}$. The positive unloading slope is the same as the positive elastic stiffness K+ 0before the member yields, and the reverse unloading slope is the same as the reverse elastic stiffness K- 0 before the member yields. The restoring force model and hysteretic principle are shown in Fig. 10. The mathematical description of the restoring force model is as follows: when loading, the load-displacement curve moves along the skeleton curve OABC, the specimen is in the elastic stage before yielding, and the loading and unloading

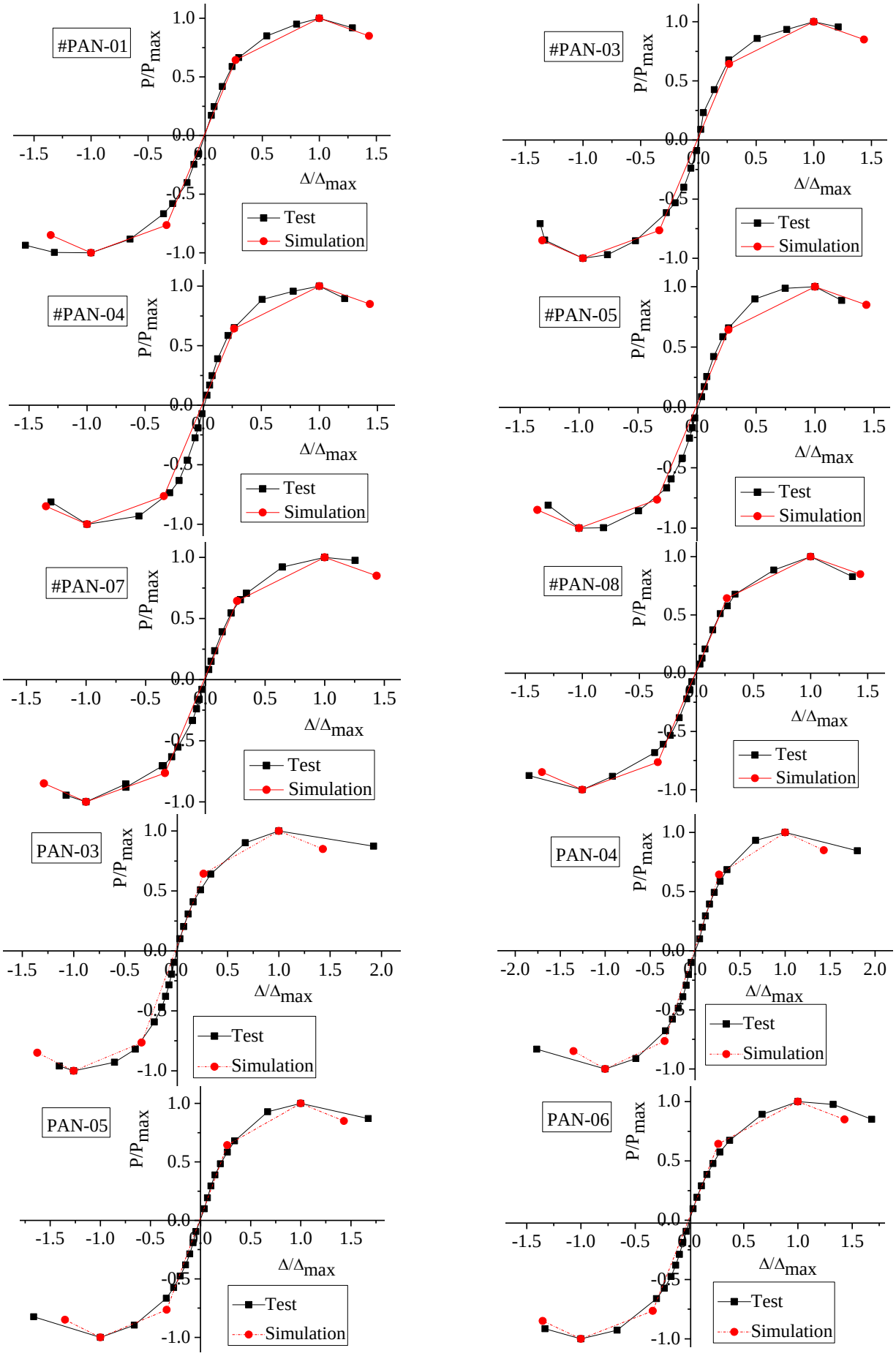

Fig. 9 Comparison of test skeleton curve and simulated skeleton curve

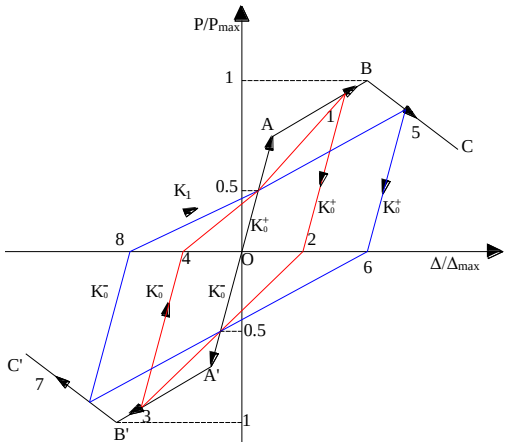

Fig. 10 Restoration force model and hysteresis rule

routes of the specimen are along the OA section (OA' section). After the specimen yields, the loading path proceeds along the direction of AB (A'B'). The positive unloading route is from 1 to 2, and the unloading stiffness is K+ 0. The reverse loading path passes through "reverse fixed point" from 2 to 3, the reverse unloading route from 3 to 4, and the reverse unloading stiffness is K- 0. The positive loading path passes through the "positive fixed point" from 4 to 1. Thereafter, the loading of the specimens continues along the skeleton curve and cycles back and forth according to the above rules until it enters the next stage. From the peak load to the failure (0.85 times the peak load), the loading path is along BC (B'C'). The loading and unloading rules at this stage are similar to those mentioned above.

5.3 Comparison of hysteretic curve

According to the established skeleton curve and hysteretic principle, the simulation results of hysteretic curves are compared and analyzed with the test results. The results are shown in Fig. 11. It can be seen from the Fig. 11 that the trend of hysteretic curves calculated by each specimen is basically consistent with the hysteretic curves obtained by the test, which shows that the proposed trilinear restoring force model can better predict the load and hysteretic performance of this kind of structure.

6. Shear bearing capacity of core zone of precast concrete joints with high strength bolt-end plate

The core area of the node plays the role of transmitting and distributing internal forces, which is also the weak part of the frame structure that withstands earthquake resistance. At present, domestic and foreign scholars have carried out a large number of experiments and theoretical studies on reinforced concrete beam-column joints, and have obtained many research results. But the unified theory has not yet formed. In this paper, bolted-end plate connections are applied in reinforced concrete structures. There are still some differences between the stress forms of the joint core area and the ordinary reinforced concrete structures. and the research on the core area of such nodes is less. Therefore, to clarify the stress mechanism of the joint core area and enrich the research of such joints, the force mechanism of the core area of precast concrete beam-column joints is analyzed in this paper. The core area of the precast concrete joint is mainly composed of core concrete, steel hoop and high-strength bolts. They exert respective material properties and provide certain contributions to the shear capacity of the node core area. Based on the research results of similar joints at home and abroad, and combined with the characteristics of the joint , the main factors affecting the shear capacity of the joint core area are the contribution of core concrete, the restraint effect of steel plate hoop and bolt pretension on core concrete, the contribution of steel plate hoop and the influence of axial pressure.

6.1 The contribution of core concrete

The core concrete stress form of the prefabricated joint core area is similar to that of the concrete filled steel tube because the stirrup is replaced by the steel hoop. The relevant experimental research and theoretical analysis show that the bearing capacity of core concrete of such joints is determined by the compressive strength of concrete baroclinic bar, and the horizontal component of the baroclinic bar is the contribution of concrete shear. According to the mechanism of baroclinic bars, the contribution of the concrete in the core area to the shear capacity can be expressed by the following formula.

$$V_{cu} = 0.8 f_{cc} ab \cos\alpha \tag{10}$$

$$a = a_b \cos\alpha + a_c \sin\alpha \tag{11}$$

$$\cos\alpha = \frac{b_c}{\sqrt{b_c^2 + h_d^2}} \tag{12}$$

Where f_{cc} is the compressive strength of confined concrete, mainly considering the restraint effect of steel plate hoop and the combined effect of bolt preload and axial force. b is the effective width of the horizontal section of the node core area. α is the angle between the line of bolt center in the compression zone and the bolt center in the corresponding tension zone and the horizontal direction. b_c is the width of column section. h_d is the distance of the outmost bolt. a_b is the distance between the center of the first row of bolts above the concrete beam and the first row of bolts below the concrete beam. The value of a_c can be obtained from equilibrium as follows

$$a_c = (0.25 + 0.8\frac{N_c}{f_{cc}A_c})b_c \tag{13}$$

$$N_c = \frac{E_c A_c}{E_s A_s + E_c A_c} N \tag{14}$$

Where N is the axial pressure applied at the top of the column; E_c is the elastic modulus of the concrete; A_c is the

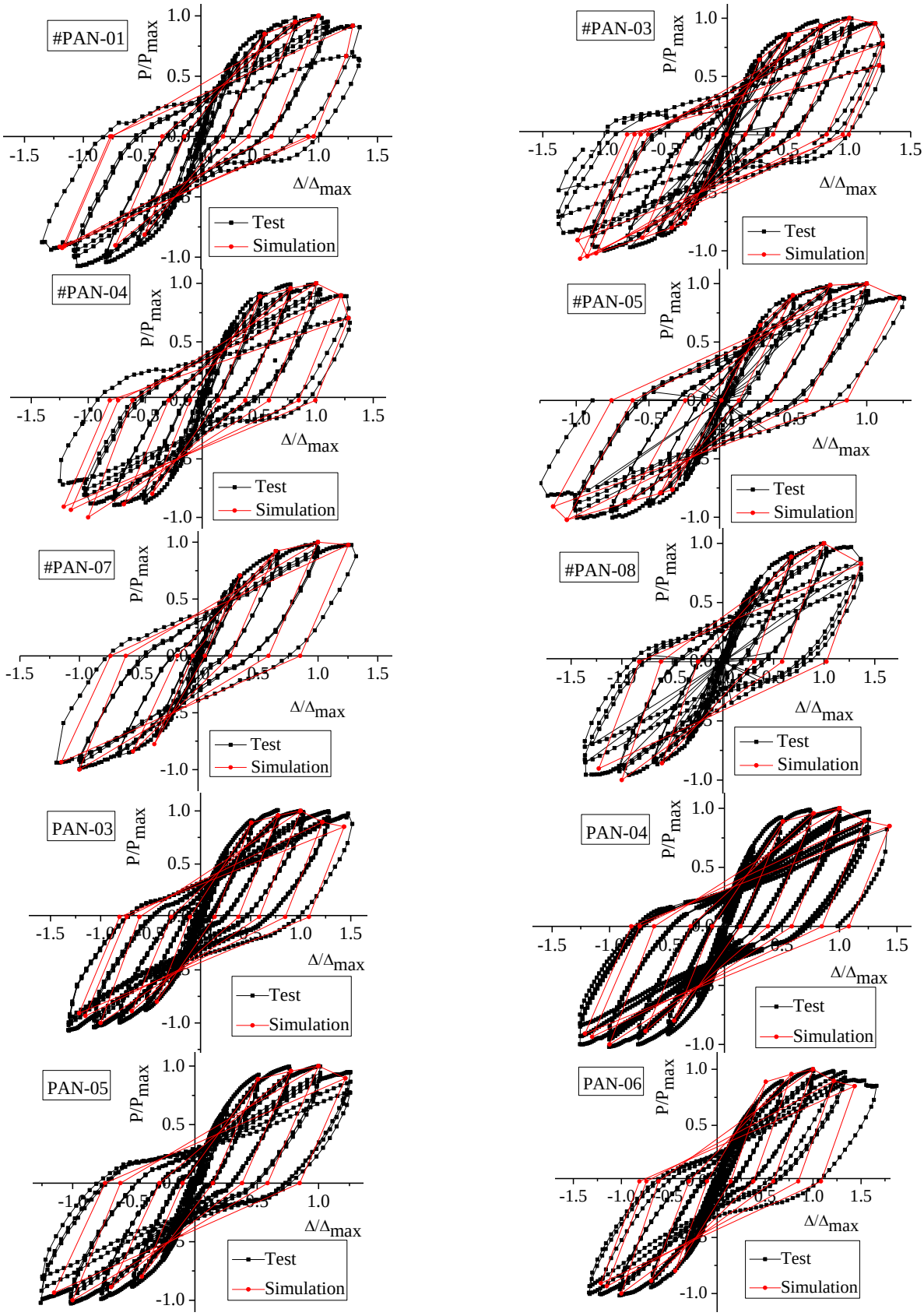

Fig. 11 Comparison of test hysteresis curve and simulated hysteresis curve

core concrete cross-sectional area; E_s is the elastic modulus of the steel plate hoop; A_s is the cross-sectional area of the steel hoop.

For the influence of bolt preload and column axial force, the improvement of the strength of core concrete can be obtained according to Kupfer-Gerstle yield criterion

(Kupfer, H.B. 1969). The strength of core concrete can be expressed as

$$f_{cc2} = -\frac{1+3.65\alpha}{(1+\alpha)^2} f_c < -0.96 f_c \tag{15}$$

$$\alpha = \sigma_1 / \sigma_2 \tag{16}$$

According to the principle of stiffness distribution, the vertical compressive stress of concrete is obtained as

$$\sigma_1 = N \bullet \frac{E_c A_c}{E_s A_s + E_c A_c} \bullet \frac{1}{A_c} \tag{17}$$

The lateral pressure produced by the bolt preload is given by

$$\sigma_2 = \frac{P}{b_c h} \tag{18}$$

Where P is the sum of the bolt preload.

From the above analysis, the compressive strength of core concrete can be calculated as follows

$$f_{cc} = f_{cc1} + f_{cc2} = (k \frac{\rho_s f_{yw}}{2 f_c} \frac{t}{B} + \frac{1+3.65\alpha}{(1+\alpha)^2}) f_c \tag{19}$$

$$\gamma = k \frac{\rho_s f_{yw}}{2 f_c} \frac{t}{B} + \frac{1+3.65\alpha}{(1+\alpha)^2} \tag{20}$$

Where γ comprehensively reflects the shear resistance of the core concrete under the constraint of steel plate hoop, bolt preload and column axial pressure.

Combined formula (10) and formula (20), the shear bearing capacity of concrete in the node core area can be expressed as

$$V_{cu} = 0.8\gamma f_c ab \cos\alpha \tag{21}$$

6.2 Contribution of steel plate hoop

The steel plate hoop in the core area of the joint not only can better restrain the core concrete and improve its compressive strength, but also have a significant effect on the shear capacity of the joint core area. Based on the coordinated deformation of steel plate hoop and concrete, the shear stress of steel plate hoop is mainly borne by side steel plate hoop. The force form of side steel hoop is shown in Fig. 12, Where σ_{SN} is the axial compressive stress from the column of the steel hoop and τ is the shear stress of the steel hoop.

Before yielding, the steel plate hoop is in the elastic stage, and the principal tensile stress is given by

$$\sigma_1 = \frac{\sigma_{SN}}{2} + \sqrt{(\frac{\sigma_{SN}}{2})^2 + \tau^2} \tag{22}$$

The principal compressive stress can be expressed as

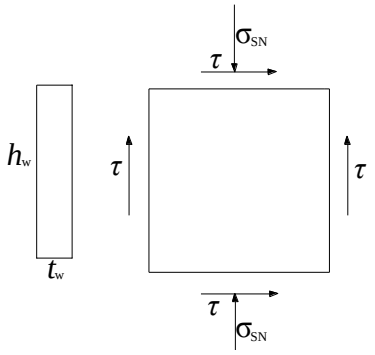

Fig. 12 Schematic diagram of stress state of steel plate hoop

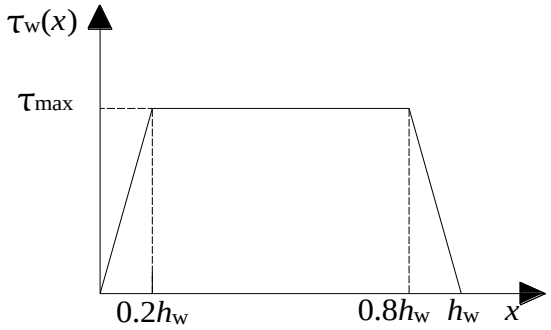

Fig. 13 Shear stress distribution diagram of steel plate hoop

$$\sigma_2 = \frac{\sigma_{SN}}{2} - \sqrt{(\frac{\sigma_{SN}}{2})^2 + \tau^2} \tag{23}$$

According to the fourth strength theory, when the limit state is reached, the condition of shear yield is obtained using the following expression:

$$\sqrt{\sigma_1^2 + \sigma_2^2 - \sigma_1\sigma_2} \le f_{ya} \tag{24}$$

Where f_{ya} is the tensile yield strength value of steel plate hoop.

Combining Eqs. (22), (23), (24), the shear yield strength of the steel plate hoop can be represented by

$$\tau_s = \frac{\sqrt{f_{ya}^2 - \sigma_{SN}^2}}{\sqrt{3}} \tag{25}$$

$$\sigma_{SN} = N \frac{E_s A_s}{E_s A_s + E_c A_c} \frac{1}{A_s} \tag{26}$$

Due to the effect of bolt preload and the bond effect between steel plate hoop and concrete, the steel plate hoop cannot fully yield. The Japanese Architectural Society considers the failure of steel hoops to yield with a reduction factor of 0.5. Relevant scholars believe that 10% steel plate hoops at both ends of the joint zone have not fully yielded (Ma, G.W. 2014, Men, J.J., Li H.J., Wang, X.D., Guan R.R. and Guo, Z.F. 2014). Combining the two cases, and taking into account the role of the bolt pre-tightening force, this paper considers that 20% of the steel plate hoops

Table 3 Comparison of experimental value and theoretical value

Literature	Specimen	Experimental value $V_{u,e}$ / kN	Theoretical value $V_{u,c}$ / kN	$V_{u,c} / V_{u,e}$
Other literature (Wu, L.Y. and Chung, L.L.2005)	FSB-6	+2663	2460	0.93
		-2694		0.92
	FSB-8	+2937	2892	0.98
		-2930		0.99
	FSB-10	+3024	3081	1.02
		-2929		1.05
Other literature (Dai, J.Z. 2012)	RCSJ6	1192	1495	1.25
	RCSJ7	1277	1463	1.15
	RCSJ8	1174	1437	1.22
	RCSJ9	1109	1257	1.13
	RCSJ10	1075	1174	1.09
	RCSJ11	1023	1159	1.13
	RCSJ12	1085	1159	1.07
mean value				1.07
standard deviation				0.99
Coefficient of variation				9.25%
This paper	#PAN-01	1018	1500	1.47
	#PAN-03	1016		1.48
	#PAN-04	1029		1.46
	#PAN-05	1020		1.47
	#PAN-07	942		1.59
	#PAN-08	986		1.52

at both ends of the joint zone do not fully reach yielding. At this time, the shear stress distribution of the steel plate hoop is shown in Fig. 13.

The shear capacity of the steel plate hoop can be expressed as

$$V_s = \int_0^{h_w} \tau_w(x) t_w \, dx = 0.46\sqrt{f_{ya}^2 - \sigma_{SN}^2} \sum t_w h_w \quad (27)$$

Combining Eqs. (21), (27), The calculation formula of the shear capacity of the precast concrete beam-column joint core area is obtained as

$$V_j = V_{cu} + V_s = 0.8\gamma f_c a b_c \cos\beta + 0.46\sqrt{f_{ya}^2 - \sigma_{SN}^2} \sum t_w h_w \quad (28)$$

The experimental values of the relevant literature and the theoretical values calculated by formula (28) are shown in Table 3.

From Table 3, it can be seen that the average value of the ratio of theoretical value to experimental value is 1.07, the variance is 0.99, and the coefficient of variation is 9.27%. The results show that the calculation results of the shear bearing capacity formula of the joint core zone presented in this paper are in good agreement with the experimental results. For the test specimens in this paper, it is reasonable that the shear bearing capacity calculated according to the proposed formula is larger than the test value. The main reason is that the plastic hinge failure occurs at the end of the beam and no shear failure occurs at the core of the joint.

7. Conclusions

- The fabricated concrete joint with high strength bolt end plate in this paper can achieve the design purpose of strong joints. From the seismic index, the fabricated joint exhibits excellent ductility and energy dissipation ability.
- Based on the experimental fitting method and the "fixed point pointing regulation", unified skeleton curve and the hysteretic principle of the fabricated concrete joint is established. The calculated restoring force model is compared with the experimental result, the result show that the coincidence of the skeleton curve and the hysteretic curve is well, which can provides a certain reference for elasto-plastic seismic response analysis of this type of structure.
- According to the analysis of the factors affecting the shear capacity of the node core area, the formula of shear capacity of the core area of the node is proposed, and the theoretical values of the formula are consistent with the experimental value, which can provide reference for theoretical research.

References

AISC (American Institute of Steel Construction) (2016), Prequalified connections for special and intermediate steel moment frames for seismic applications. ANSI/AISC 358-16, Chicago, IL.

CECS:2013 (2013), Technical specification for frame structure of confined RC columns and composite beams.

Chen, W.W. and Li, S.C (2014), "Study on restoring force model of steel-concrete composite joints with extended end-plate connections", *World Earthquake Engineering*., **30**(1), 105-113.

Cheng, P., Miao, X.Y. and Xu, J.W. (2015), "Experimental study on a new type of column-to-beam joints in assembled reinforced concrete frame structures", *Industrial Construct.*, **45**(12), 94-98. https://doi.org/10.13204/j.gyjz201512017

Dai, J.Z. (2012), "Experimental Study on Seismic Behaviour of Prefabricated Reinforced Concrete Column to Steel Beam Hybrid Joints", Huaqiao University, Quanzhou, China.

Fan, L. (2010), "Investigation on behavior factor of jointed precast concrete frame structures", *Civil Eng. J.*, **43**, 131-136. https://doi.org/10.15951/j.tmgcxb.2010.s2.035

GB50017-2017(2017), Code for design of steel structures.

Guan, D.Z., Guo, Z.X., Yang, H. and Yang, S. (2018), "Restoring force model of precast beam-column connections incorporating beams with grooves and anchored bottom longitudinal bars", *J. Southeast University*, **48**(05), 44-50. https://doi.org/CNKI:SUN:DNDX.0.2018-05-007

He, Y.B. Huang, P., Guo, J., Zhou, H.B., Li, Y. and Li, Y. (2012), "Experimental study on seismic behavior of steel-reinforced concrete square column and steel beam joint with bolted end-plate", *J. Building Struct.*, **33**(7), 116-125. https://doi.org/10.14006/j.jzjgxb.2012.07.014

Jiang, H.T., Li, Q.N., Jiang, W.S. and Zhang, D.Y. (2016), "Study on seismic performance of connection joint between prefabricated prestressed concrete beams and high strength reinforcement-confined concrete columns", *Steel Compos. Struct.*, **21**(2), 343-356. https://doi.org/10.12989/scs.2016.21.2.343.

Kupfer, H.B. (1969), "Nonlinear behavior of concrete under biaxial stress", *J. Eng. Mech. Division ASCE.*, **99**(8), 853-866. https://doi.org/10.14359/7388

Li, X.M., Gao, R.D. and Xu, Q.F. (2013), "Experimental study on high ductile joints for precast RC frame", *J. Central South University (Science and Technology)*., **44**(8), 3453-3463.

Liao, X.D., Hu, X., Ma, R.Q. and Xue,W.C.(2016), "Experimental studies on seismic performance of monolithic precast prestressed concrete frame interior connectionsunder high axial compression ratio", *J. Build. Struct.*, **37**(10), 82-89. https://doi.org/10.14006/j.jzjgxb.2016.10.010

Liu, R.R. (2015), "Experimental Study on Seismic Performance of Prestressed Assembling Frame Model of Intermediate Node Structure", Hebei United University, Tangshan, China.

Ma, G.W. (2014), "Study on the combination of nodes connected composite beams and CCSHRC column bolted end plate", Xi'an University of Architecture and Technology, Xi'an, China.

Men, J.J., Li H.J., Wang, X.D., Guan R.R.and Guo, Z.F. (2014), "Research on shear bearing capacity of reinforced concrete column-steel beam composite joint", *Build. Struct*., **44**(6), 74-78. https://doi.org/10.19701/j.jzjg.2014.06.018

Mohammad, Y., Amir, Ti. and Seyed, M.Z. (2016), "Experimental and numerical evaluation of proposed precast concrete connections", *Struct. Concrete*., **17**(6), 959-971. https://doi.org/10.1002/suco.201500168

Parastesh, H., Hajirasouliha, I. and Ramezani, R. (2014), "A new ductile moment-resisting moment-resisting connection for precast concrete frames in seismic regions: An experimental Investigation", *Eng. Struct.*, **70**, 144-157. https://doi.org/10.1016/j.engstruct.2014.04.001

Peng, Z. Dai S.B. Liu J.X. and Zhang, Y.C. (2016), "Experimental Research on Seismic Performance of Extended-end-plate Connecting Joint Between T-shaped Concrete-filled Steel Tubular Composite Column and Reinforced Concrete Beam", *J. Sichuan University (Engineering Science Edition)*., **48**(8), 70-77. https://doi.org/10.15961/j.jsuese.2016.04.010

Rattapon, K. and Chayanon, H. (2018), "Seismic performance of interior precast concrete beam-column connections with T-section steel inserts under cyclic loading", *Earthq. Eng. Eng. Vib.*., **17**(2), 355-369. https://doi.org/10.1007/s11803-018-0446-9

Tartaglia R., D'Aniello M. and Rassati G.A. (2019), "Proposal of AISC-compliant seismic design criteria for ductile partially-restrained end-plate bolted joints", *J. Construct. Steel Res.*., **159**, 364-383. https://doi.org/10.1016/j.jcsr.2019.05.006

Tartaglia R., D'Aniello M., Rassati G.A., Swanson J.A. and Landolfo R. (2018), "Full strength extended stiffened end-plate joints: AISC vs recent European design criteria", *Eng. Struct.*, **159**, 155–171. https://doi.org/10.1016/j.engstruct.2017.12.053

Tartaglia R., D'Aniello M., Zimbru M. and Landolfo R. (2018), "Finite element simulations on the ultimate response of extended stiffened end-plate joints", *Steel Compos. Struct*., **27**(6), 727-745. https://doi.org/10.12989/scs.2018.27.6.727

Wang, L., Yan, S.J., Zheng, Y. and Zhang C.L. (2014), "Tests on seismic behavior of joints in steel frame with steel-concrete composite beams", *J. Harbin Institute of Technol.*., **46**(4), 1-6. https://doi.org/10.11918/j.issn.0367-6234.2014.04.001

Wu, L.Y. and Chung, L.L. (2005), "Seismic behavior of bolted beam-to-column connections for concrete filled steel tube", *J. Construct. Steel Res.*, **61**(10), 1387-1410. https://doi.org/10.1016/j.jcsr.2005.03.007.

Yu, J.B. and Guo, Z.X. (2017), "Experimental study on new precast frame connections under low cyclic loading", *Earthq. Eng. Eng. Dynam.*, **37**(05), 141-147. https://doi.org/CNKI:SUN:DGGC.0.2017-05-016/

Zeng, L. (2008), "Research on seismic behaviors and design method of steel reinforced high strength and high performance concrete frame joints", Xi'an University of Architecture and Technology, Xi'an, China. https://doi.org/10.7666/d.d196369.

Zenunović, D. and Folić R. (2012), "Models for behavior analysis of monolithic wall and precast or monolithic floor slab connections", *Eng. Struct.*, **40**, 466-478. https://doi.org/10.1016/j.engstruct.2012.03.007.

Zhang, X.H., Ma, G.W., Ma, H.W. and Jiang, W.S. (2014), "Experiment on End Plate Bolted Connection Node of SC beam and CCSHRC Column", *J. Architect. Civil Eng.*, **31**(2), 51-56. https://doi.org/10.3969/j.issn.1673-2049.2014.02.010.

PL